

# Evaluation of scintillometry measurements of fluxes of momentum and sensible heat in the roughness sublayer

Hirofumi Sugawara<sup>1</sup> · Atsushi Inagaki<sup>2</sup> · Matthias Roth<sup>3</sup> · Manabu Kanda<sup>2</sup>

Received: 23 March 2015 / Accepted: 30 June 2015 / Published online: 19 August 2015  
© Springer-Verlag Wien 2015

**Abstract** Scintillometer measurements of turbulent fluxes of momentum and sensible heat in the roughness sublayer over a regular array of cubes in an outdoor environment were tested with direct measurement from sonic anemometers. The dissipation rate,  $\varepsilon$ , and temperature structure parameter,  $C_T^2$ , obtained from the scintillometer agreed well with those from four sonic anemometers located along the scintillometer path. The fluxes measured by the scintillometer also corresponded well to those from the line-averaged eddy covariance approach, although this agreement was greatly influenced by the choice of the zero-plane displacement length and the form of the similarity function used in the scintillometer software. A guide for choosing the appropriate similarity function for the urban roughness sublayer is proposed.

## 1 Introduction

Turbulent flux measurements over building canopies are essential for a range of real-world applications which include the better understanding of the energetics of the urban heat island, cycling of trace gases between the urban surface and the atmosphere, and the dispersion of pollutants. Eddy covariance (EC), which analyzes high-frequency wind and scalar data, is

the only approach which measures turbulence directly and has been used extensively in the majority of past urban energy balance and turbulence research (Roth 2000; Moriwaki and Kanda 2006; Christen et al. 2009). A less popular but promising alternative approach is scintillometry (SL) which measures small fluctuations of the refractive index of air along a light beam. It derives heat and momentum fluxes through the application of Monin-Obukhov similarity theory (MOS) and has the following advantages compared to EC:

1. SL measures the line average of a flux along its optical path and can cover an area 3.5 times larger than the footprint of an EC sensor in unstable conditions (Kanda et al. 2002; hereafter KA02).
2. EC can be greatly influenced by flow distortion caused by obstacles in the immediate vicinity of the sensor; SL is less affected because its highest sensitivity is in the center of the optical path (Fig. a1 in Scintec 2008).
3. SL is more suitable than EC in the case of a stable atmosphere because of its shorter averaging period and the smaller size of the measured eddies (Hartogensis et al. 2002).

Points 1 and 2 in particular make SL an attractive option for use in the roughness sublayer (RSL) which is characterized by large spatial variations in its flow and scalar characteristics, and where EC is inadequate for measuring an area average.

Although SL has been applied above the urban RSL (e.g., Lagouarde et al. 2005; Ward et al. 2014), only very few studies so far have attempted to use it in the RSL. Meijninger et al. (2002) validated SL below the blending height (upper boundary of the RSL) over flat and heterogeneous surfaces covered by different types of vegetation. They showed that the sensible heat flux from SL agrees well with the area-averaged flux from four eddy covariance sensors located within the SL footprint. The study, however, focused on a thermally heterogeneous RSL with

✉ Hirofumi Sugawara  
hiros@nda.ac.jp

<sup>1</sup> Department of Earth and Ocean Sciences, National Defense Academy of Japan, Yokosuka, Japan

<sup>2</sup> Department of International Development Engineering, Tokyo Institute of Technology, Tokyo, Japan

<sup>3</sup> Department of Geography, National University of Singapore, Singapore, Singapore

little spatial variability in aerodynamic surface properties. It also showed that fluxes derived by SL strongly depend on the choice of the displacement length and the function of the Monin-Obukhov similarity theory used in the SL equations, both of which are likely unique to a particular location if the observations are within the RSL. Roth et al. (2006) (hereafter RO06) compared SL and EC approaches in an urban RSL. They showed good agreement for the dissipation rate,  $\varepsilon$ , and temperature structure parameter,  $C_T^2$ , with one EC sensor located at the SL midpoint which, however, is not sufficient to guarantee spatial representativeness in the RSL. A more rigorous test over an aerodynamically rough surface is therefore needed.

The objective of the present study is to validate raw SL data ( $\varepsilon$  and  $C_T^2$ ) and fluxes of sensible heat and momentum in an aerodynamically rough RSL over a physical scale model using an array of four sonic anemometers. In principle, MOS theory cannot be applied close to inhomogeneous surfaces. However, a number of previous studies have shown the possible application of urban forms of MOS in the RSL (RO06, KA02) which were also tested in the present study.

## 2 Site description and measurements

The Comprehensive Outdoor Scale Model for urban climate (COSMO) experimental site was used for the measurements. At the COSMO site, 512 concrete cubes ( $1.5 \times 1.5 \times 1.5$  m) were arranged in a regular grid pattern with 1.5-m spacing on a flat concrete plate resulting in an obstacle plan area density of 0.25. All surfaces were painted dark gray. The configuration of cubes and sensors is shown in Fig. 1. Flat, bare soil extends  $>500$  m upwind of the site (toward NW). More details on the COSMO site are available in Kanda et al. (2007), and turbulence characteristics are described in Inagaki and Kanda (2008) and Roth et al. (2015).

The same measurement setup as in Roth et al. (2015) was used but complemented with a bichromatic, small-aperture scintillometer (Scintec, SLS-20). The SLS-20 with a standard software provided 1-min value of  $\varepsilon$  and  $C_T^2$  along a 48-m path which were further averaged over 30 min. Four sonic anemometers (Kaijo, TR90AH) installed along the scintillometer beam measured turbulence statistics and fluxes. This particular anemometer has a span width of 5 cm, signals were sampled at 50 Hz, and statistics calculated for 30-min periods.

Four anemometers were placed to represent one roughness unit (one roof-top and canyon pair, respectively) to sample the full spatial variability of the flow which is assumed to repeat itself across the entire array. The beam of the scintillometer was located to coincide with the sonic anemometers. The anemometers were installed at the center of the cube array and scintillometer path considering with its peak sensitivity (Fig. 1). Measurements were conducted either above the center of cubes (referred to as “roof-top” in the following) or canyon (referred

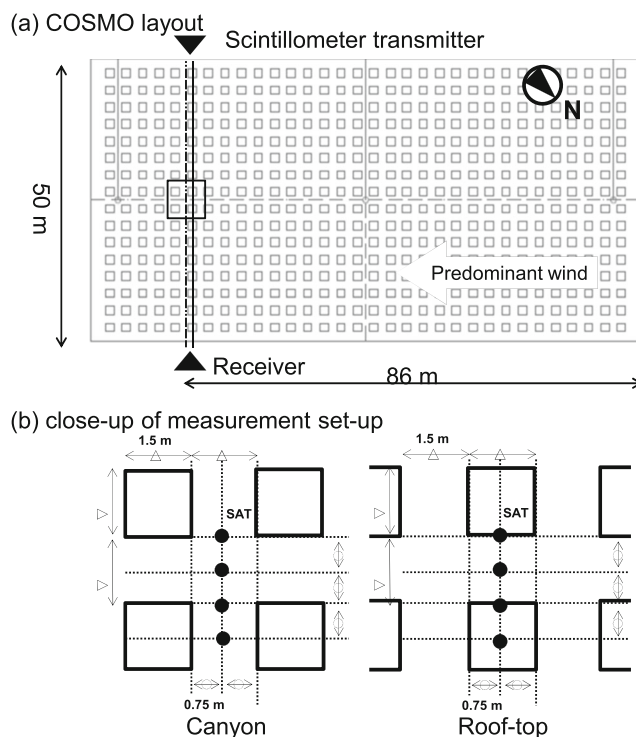


**Fig. 1** Experimental site and sensor locations. *Squares* are cubes. *Filled triangles and circles* show the locations of the scintillometer (transmitter and receiver) and sonic anemometers (SAT), respectively. **b** is close-up of rectangular in **a** for sensors above canyon (*left*) and roof-tops (*right*), respectively

to as “canyon”), respectively, at heights of  $1.0H$  ( $1.125H$  in the case of the roof-top location),  $1.25H$ ,  $1.5H$ , and  $2H$ , where  $H$  is the cube height. Two scintillometers were used, taking simultaneous measurements at two different heights with four sonic anemometers each. The two scintillometers were compared against each other before the experiment and showed good agreement ( $R = 0.97$  and  $0.98$  for  $\varepsilon$  and  $C_T^2$ , respectively). The relative performance of the sonic anemometers was also investigated, and  $u_*$  values, for example, agreed within  $0.011 \text{ m s}^{-1}$  of each other (Inagaki and Kanda 2008). The top of the RSL at the COSMO site is found between  $1.5$  and  $2.0H$  as derived from the spatial variation of mean and fluctuating velocity components (Inagaki and Kanda 2008). The present measurements therefore cover the area between the top of the roughness elements and top of the RSL.

Measurements were taken during the dry season (February to April 2006 and April 2007; average vapor pressure =  $6.3 \text{ hPa}$ ) when the concrete surface was dry, to minimizing the influence of water vapor on the  $C_n^2$  measurements. The following quality control steps were further applied: (1) mean wind direction perpendicular to the SL path within  $\pm 45^\circ$ , (2) data availability ratio of SL ( $NOK$ )  $> 80\%$ , and (3) exclusion of runs with suspicious spikes in sonic anemometer data ( $\sigma_u > 2 \text{ m s}^{-1}$ ,  $\sigma_w > 1 \text{ m s}^{-1}$ , or  $(\overline{u'w'}) > 0 > 0$ ), where  $\overline{u'w'}$  is the momentum flux. The number of remaining runs available for

analysis ranged between 6 (roof-top, 1.5H) and 59 (canyon, 1.5H) (detail list will be shown in Tables 2 and 3) covering mostly near-neutral to unstable conditions.

The zero-plane displacement length ( $d$ ) is one of the input variables need to derive sensible heat and momentum fluxes using SL.  $d$  was evaluated using four independent methods: (1) morphometric approach, which relates  $d$  to surface roughness indices. Here, we used equations from Bottema (1997) and Macdonald et al. (1998) applied to the LES model results from Kanda et al. (2013) where friction velocity  $u_*$  is explicitly calculated from the momentum balance. (2) Temperature variance method where MOS is applied to the measured variance of temperature, and  $d$  is determined as the best fit to all runs (Rotach 1994; Toda and Sugita 2003). (3) Scintillometer heat flux method which determines  $d$  as the scintillometer-measured heat flux that agrees at two heights assuming a constant flux layer (KA02) using the MOS function developed by KA02 and SL data at 1.5H and 2.0H over the canyon location. (4) Aerodynamic approach using the neutral wind speed profile (Inagaki and Kanda 2008). Table 1 shows very good agreement among the four methods, although there was considerable variation in the morphometric results depending on the equation used. A value of  $d = 1.15$  m was eventually adopted for the present analysis.

### 3 Analytical procedure

The principles of scintillometry can be found in Thiermann and Grassl (1992) (hereafter TG92). The scintillometer used in the present study derives  $\epsilon$  and  $C_T^2$  from intensity fluctuations of a transmitted signal along two parallel light beams. These variables were compared to those obtained from the spectral energy density in the inertial subrange of turbulence spectra measured by the sonic anemometers:

$$\epsilon = (nS_w(n))^{3/2} (2\pi n/U) A^{-3/2} \tag{1}$$

$$C_T^2 = 4\beta_1 (nS_T(n)) (2\pi n/U)^{2/3} B_T^{-1} \tag{2}$$

**Table 1** Displacement length  $d$  at COSMO site

Method		$d$ [m]
Morphometric	Bo	1.16
	Ma	0.72
	Ka	1.19
Variance		1.15
Scintillometer		1.15 ( $\pm 0.24$ )
Neutral wind speed profile		1.25

See text for more details

Bo, Ma and Ka were calculated using equations from Bottema (1997), Macdonald et al. (1998), and Kanda et al. (2013), respectively

where  $n$  is the natural frequency ( $s^{-1}$ ),  $S_w$  and  $S_T$  are the spectral energy density of vertical wind speed,  $w$  and temperature,  $T$ , respectively,  $U$  is the mean wind speed.  $A = 0.73$ ,  $B_T = 0.78$ , and  $\beta_1 = 0.86$ .  $S_w$  were found to exhibit the  $-2/3$  slope expected in the inertial subrange, similar to past research at the same location (Inagaki and Kanda 2008; Roth et al. 2015). The  $-2/3$  slope extended over a narrower frequency range for  $S_T$  compared to  $S_w$  ( $n = 0.3-3$  and  $0.5-10 s^{-1}$ , respectively) which may be due to more fragile in the sonic temperature measurement against the white noise compared in the near-neutral stratification. The average of  $\epsilon$  ( $C_T^2$ ) from the four sonic anemometers along the SL beam was used as the comparison standard.

SL calculates the sensible heat and momentum flux using the nondimensional forms of  $\epsilon$  and  $C_T^2$  given by the following:

$$\phi_\epsilon = \frac{kz'\epsilon}{u_*^3} \tag{3}$$

$$\phi_{CT} = \frac{C_T^2 (kz')^{2/3}}{T_*^2} \tag{4}$$

where  $u_*$  is the friction velocity,  $T_*$  is the friction temperature,  $k$  is the von Karman constant ( $=0.4$ ), and  $z'$  is the effective height ( $=z - d$ ).  $\phi_\epsilon$  and  $\phi_{CT}$  are calculated using MOS theory, and several forms of MOS equations are available for unstable conditions. The following equations were developed by RO06 for the RSL above a canyon:

$$\phi_\epsilon(\zeta) = 0.38 + 1.9|\zeta|^{0.8} \tag{5}$$

$$\phi_{CT}(\zeta) = 3.44 \left( 0.8(1.1-4\zeta)^{-0.75} \right) \left( 0.38 + 1.9|\zeta|^{0.8} \right)^{-1/3} \tag{6}$$

and roof-tops:

$$\phi_\epsilon(\zeta) = (0.93-5.4\zeta)^{-1.1} - 2\zeta \tag{7}$$

$$\phi_{CT}(\zeta) = 3.44 \left( 1.42(-0.03-24\zeta)^{-0.46} \right) \left( (0.93-5.4\zeta)^{-1.1} - 2\zeta \right)^{-1/3} \tag{8}$$

where  $\zeta = z'/L$ ,  $L$  is the Obukhov length. Equations for above canyon are valid for  $-5 < \zeta \leq -0.01$ , and those for a roof-top are valid for  $-2 < \zeta \leq -0.001$  (for  $\epsilon$ ) and  $-2 < \zeta \leq -0.005$  ( $C_T^2$ ), respectively. KA02 developed MOS equations based on measurements in the suburban surface layer valid for  $-3 < \zeta < 0$ :

$$\phi_\epsilon(\zeta) = (1-10.5\zeta)^{-1} \tag{9}$$

$$\phi_{CT}(\zeta) = 4\beta_1 \left( 0.68(1-9.69\zeta)^{-1/2} \right) \left( (1-10.5\zeta)^{-1} - \zeta \right)^{-1/3} \tag{10}$$

The original equations from TG92 developed for unstable conditions for flat and homogeneous surfaces and used in the SLS-20 software are also tested below:

$$\phi_\varepsilon(\zeta) = (1-3\zeta)^{-1}-\zeta \quad (11)$$

$$\phi_{CT}(\zeta) = 4\beta_1(1-7\zeta + 75\zeta^2)^{-1/3} \quad (12)$$

In the following, the sensitivity of the SL approach to the choice of  $d$  and the various MOS functions listed above is evaluated.

#### 4 Test of $\varepsilon$ and $C_T^2$

Dissipation rates derived from SL ( $\varepsilon_{SL}$ ) are compared to those from the sonic anemometer ( $\varepsilon_{EC}$ ) at the canyon location in Fig. 2. Tables 2 and 3 summarize the regression statistics from both locations. Generally very good agreement between  $\varepsilon_{SL}$  and  $\varepsilon_{EC}$  is observed, where any disagreement is within the spatial or temporal variation of the measurements (Fig. 2). However, the data also demonstrate a tendency for SL to slightly underestimate  $\varepsilon$ , in particular at 2.0H and 1.0H. The underestimation in the present study is probably partly due to instrumental limitations in the SL approach. The scintillometer has a lower limit for inner scale ( $l_0$ ) measurements which translates into an upper limit for  $\varepsilon$ , given the following relationship:

$$\varepsilon = \nu^3 \left( \frac{7.4}{l_0} \right)^4 \quad (13)$$

where  $\nu$  is the kinematic viscosity of air. The upper limit for  $\varepsilon$  becomes smaller as the path length becomes shorter. Using a path length of 48 m, the maximum dissipation rate that can be measured is  $\sim 0.06 \text{ m}^2 \text{ s}^{-3}$  (Scintec 2008). This will reduce the average if there are areas along the SL beam with values  $>0.06 \text{ m}^2 \text{ s}^{-3}$  which cannot be detected.

Other studies have also reported similar underestimation (RO06; Hartogensis et al. 2002), however, with reasons which may not be applicable to the present study. Sensor vibration has been highlighted by De Bruin et al. (2002) but can be neglected here because wind speed was  $<3 \text{ m s}^{-1}$ . Another possibility could be the unintended displacement of the two beams in the SLS-20 which can differ between individual sensors. Use of an incorrect value for that length in the SL calculation may result in a significant change in  $\varepsilon$  (Hartogensis et al. 2002; Van Kesteren et al. 2013). In the present study, however, the underestimation was similar for both SLS-20 units, and  $\varepsilon$  during a pre-experiment comparison was in good agreement (see Sect. 2).

Vertical wind speed was used to estimate  $\varepsilon$  in Fig. 2. Scatter plots and regression statistics for  $\varepsilon$  using the horizontal wind components are very similar (not shown). The SL approach overestimates  $C_T^2$  at the lower two measurement levels at the canyon location (Fig. 2 and Table 3) and all heights at the rooftop location (Table. 3). Hartogensis et al. (2002) found similar

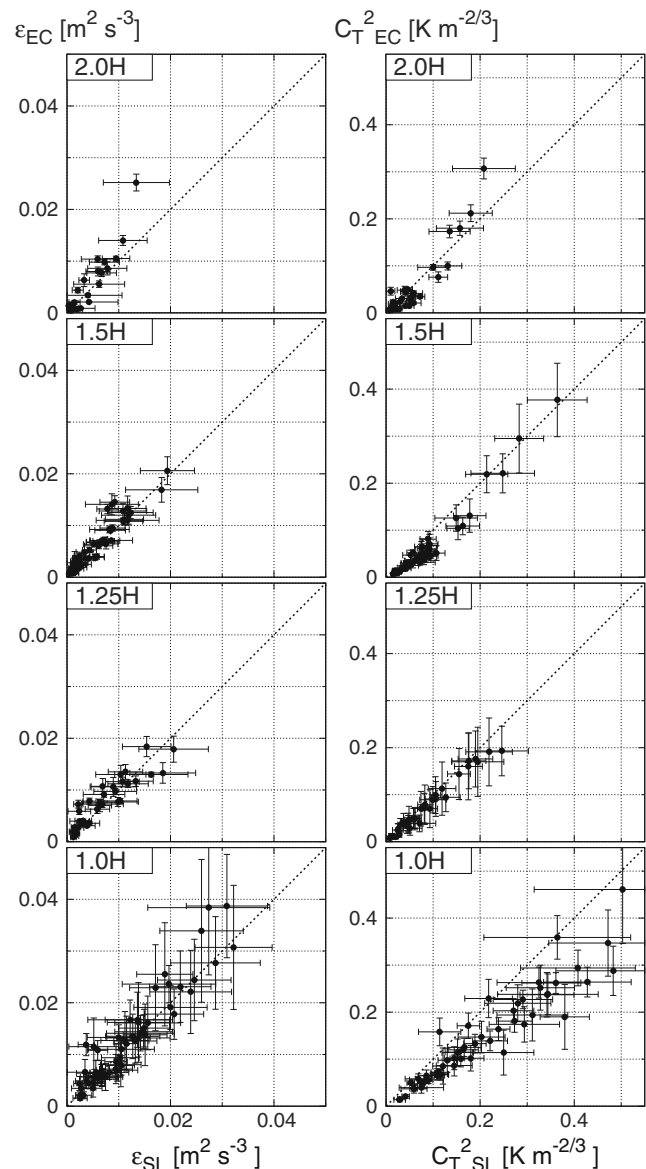


**Fig. 2** Scatterplots of SL and EC (average of four sonic anemometers) measurements of (left)  $\varepsilon$  and (right)  $C_T^2$  at four heights (bottom to top 1.0H, 1.25H, 1.5H, and 2H) at the canyon location. Mean value (points) and standard deviation (error bars). Error bars for SL reflect time variation of individual 1-min values over 30 min and for EC spatial variation across the four sonic anemometers used, respectively. The  $\varepsilon$  values for EC are obtained from the  $w$  spectrum

results; however, they calculated reference  $C_T^2$  not from spectra but the spatial correlation in temperature fluctuations at two points. The following reasons can possibly explain the observed differences:

1. In the SL procedure,  $C_T^2$  is determined from light fluctuations of a single beam ( $B_1$ ) and  $l_0$ . Since  $C_T^2$  is positively correlated to  $l_0$ , the instrumental limit of  $l_0$  noted above can result in overestimating this variable and hence  $C_T^2$ . A sensitivity analysis showed that a 10 % underestimation in

**Table 2** Regression statistics between SL and EC for dissipation values ( $\epsilon$ )

Location	<i>a</i>	<i>b</i> [m <sup>2</sup> s <sup>-3</sup> ]	Bias [m <sup>2</sup> s <sup>-3</sup> ]	RMS [m <sup>2</sup> s <sup>-3</sup> ]	<i>N</i>
Roof-top 2H	1.76	-0.001	-0.005	0.008	17
Roof-top 1.5H	1.57	-0.002	-0.001	0.003	6
Roof-top 1.25H	0.93	0.005	-0.004	0.008	18
Roof-top 1.125H	1.27	-0.001	-0.003	0.005	25
Canyon 2H	1.49	-0.001	-0.002	0.004	58
Canyon 1.5H	1.04	0.000	-0.001	0.002	59
Canyon 1.25H	0.81	0.002	-0.001	0.002	34
Canyon 1.0H	1.10	-0.000	-0.001	0.003	58
Average			-0.002	0.004	

Coefficients *a* and *b* are fitted to  $\epsilon_{EC} = a\epsilon_{SL} + b$ ; bias = mean of  $\epsilon_{EC} - \epsilon_{SL}$ ; RMS = root mean square of  $\epsilon_{EC} - \epsilon_{SL}$ ; *N* = number of 30-min runs. Values of  $\epsilon$  by EC are obtained from the *w* spectrum

- $l_0$ , which correspond to the degree of overestimation in  $\epsilon$  in Fig. 2, causes an 18 % underestimation in  $C_T^2$ .
- The size of the smallest turbulent eddies sensed by the EC and SL approach is different. The sonic anemometer measures temperature fluctuation using a transmitter and detector pair aligned vertically (normal to the mean wind). Assuming a wind speed of 1 m s<sup>-1</sup> and sampling rate of 50 Hz, the smallest eddy size sensed has a diameter of 2 cm (1 m s<sup>-1</sup> times 0.02 s), which compares to 0.1 cm (beam aperture) for the SL. This difference could influence the comparison in Fig. 2 if the eddy size in either measurement is outside the inertial subrange. It is possible that turbulent eddies with dimensions of a few centimeters do not achieve isotropy at the COSMO site because the inertial subrange is shifted to higher frequencies compared to that over a flat homogeneous surface. The same argument cannot be applied to  $\epsilon$  whose measurement principles are different between temperature and wind speed in EC.
  - The sonic anemometers are located at the mid-point of the SL path. Although the SL has its highest sensitivity in the middle of its measurement path, it also senses the flow near the edge of the path, where horizontal advection from

outside the COSMO site could produce a larger temperature gradient.

- The SL measurement becomes more sensitive to the form of the spectrum of the refractive index as the path becomes shorter (Hartogensis et al. 2002). The model of Hill (1978) which is included in the SLS-20 software was used in the present study. Testing other models was beyond the scope of the present study, although Fig. 1 in Hartogensis et al. (2002) suggests that this may solve the  $C_T^2$  overestimation (e.g., Frehlich 1992).

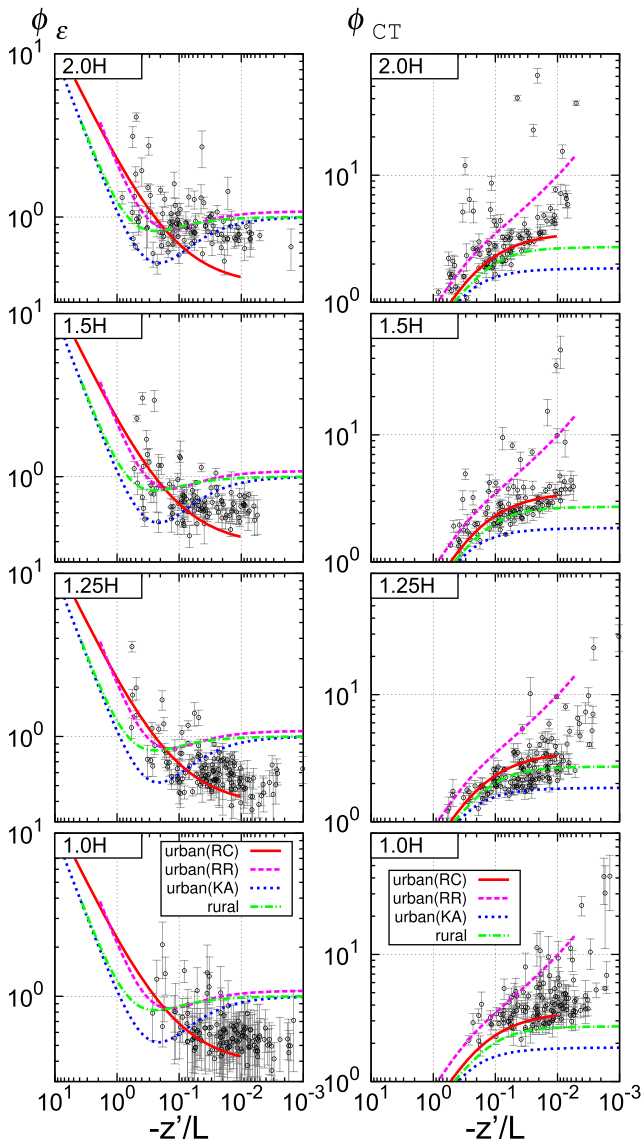
### 5 MOS function

Figure 3 shows  $\phi_\epsilon$  and  $\phi_{C_T^2}$  based on the EC measurements above the canyon, together with a selection of urban MOS functions and a rural reference (Eqs. 5–12). Measured  $\epsilon$  and  $C_T^2$  were averaged horizontally across the four sonic anemometers, and then normalized with averaged normalization variables. At the lowest two levels corresponding to the height of the obstacles and just above, the data for  $\phi_\epsilon$  agree well with the empirical function for a similar canyon location obtained by RO06. At  $z = 1.5H$ , the overall shape of the RO06 fit is followed, but near-neutral values are larger and between the urban and rural reference curves. At  $z = 2.0H$ , the observations agree better with the rural reference rather than the urban curves. This result demonstrates the transition from the RSL to the inertial sublayer. On the other hand, such a shift could not be found for the roof-top locations where the data for  $z'/L > -0.1$  at all heights are scattered between the urban and rural references (Fig. 4).

This result can be understood by considering the structure of the RSL above regular cube roughness. Roth et al. (2015) found two internal sublayers which developed over cube arrays (Fig. 5). Sublayer 1 is generated at the upwind edge of a cube, develops over the top of the cube, and is characterized by decreased Reynolds stress. This is due to the damping of vertical motions near the solid roof-top surface which causes  $\phi_\epsilon$  at the roof-top location to be close to that over a flat surface. Note that the MOS function for the roof-top in R06 is

**Table 3** Same as Table 2 but for  $C_T^2$

Location	<i>a</i>	<i>b</i> [K m <sup>-2/3</sup> ]	Bias [K m <sup>-2/3</sup> ]	RMS [K m <sup>-2/3</sup> ]	<i>N</i>
Roof-top 2H	0.78	-0.028	0.079	0.137	23
Roof-top 1.5H	0.93	0.001	0.003	0.005	6
Roof-top 1.25H	0.54	0.008	0.075	0.154	16
Roof-top 1.125H	0.70	-0.008	0.041	0.045	25
Canyon 2H	1.23	-0.016	0.003	0.027	32
Canyon 1.5H	1.00	-0.023	0.022	0.027	59
Canyon 1.25H	0.88	-0.001	0.011	0.017	34
Canyon 1.0H	0.73	-0.003	0.058	0.075	54



**Fig. 3** Normalized (*left*) dissipation rate ( $\phi_\varepsilon$ ) and (*right*) temperature structure parameter ( $\phi_{CT}$ ) as a function of  $z'/L$  calculated from EC measurements (average of four sonic anemometers) at four heights (*bottom to top* 1.0H, 1.25H, 1.5H, and 2H) at the canyon location. Also plotted are urban MOS functions from RO06 (RC canyon case,  $z = 1.01H$ ; RR rooftop case,  $z = 1.32H$ ), KA02 (KA  $z = 2.62H$  and  $3.8H$ ) and rural reference from TG92 (*rural*). Error bars reflect the spatial variation of  $\phi_\varepsilon$  across the four sonic anemometers used

close to that for the rural reference, indicating that the internal boundary layer above the roof-top should be similar to that over a homogeneous flat surface. Sublayer 2 develops at the downwind edge of the cube and includes the space above the canyon. The measurement levels at 1.0, 1.25, and 1.5H above the canyon were located in sublayer 2. Here,  $\phi_\varepsilon$  was significantly less than unity, indicating higher local shear production than dissipation. This agrees with the large Reynolds stress in this sublayer shown in Roth et al. (2015). These sublayers are generated at the edges of cubes and are broadened perpendicular to the mean wind direction by turbulent diffusion and

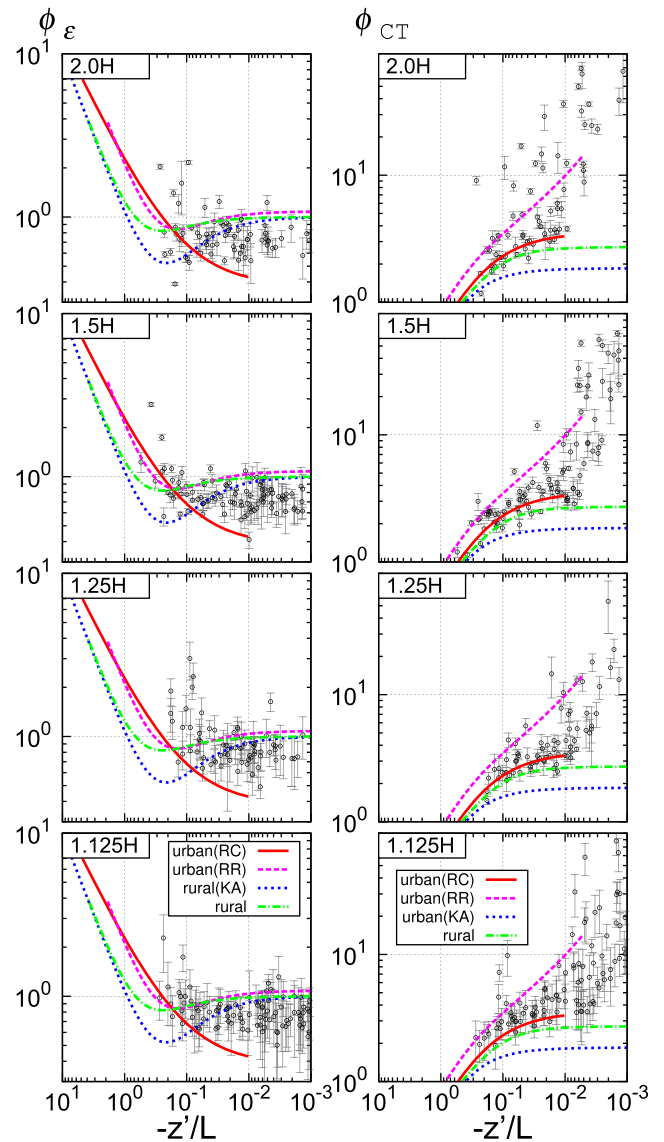


**Fig. 4** Same as Fig. 3 but for the roof-top location

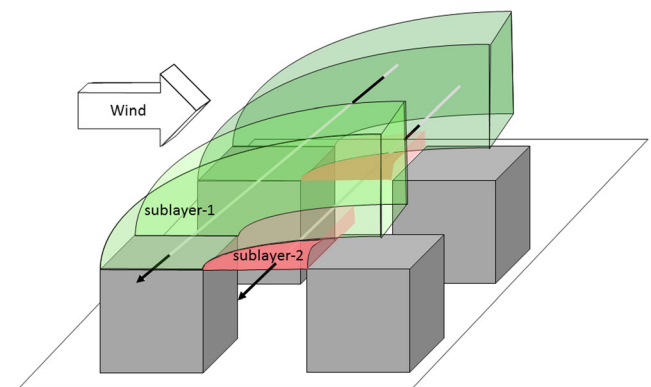


**Fig. 5** Schematic illustration of the internal boundary layer over a regular array of cubes. Arrows indicate location of SL beam for a canyon and roof-top location, respectively. Aspect ratio of cubes and sublayers are not to scale

fluctuations of the wind direction. This broadening makes the sublayers spatially representative along the SL path.

The present canyon measurements for  $C_T^2$  broadly agree with those from the rural reference and the canyon function from RO06 at both locations and all levels for  $0.01 < -z'/L < 1$ . However, there are a number of large values especially at  $z > 1.5H$  which may be due to advection of horizontal temperature variations. Large horizontal temperature gradients close to the surface produced by the proximity of sunlit and shaded surfaces may also be the reason for values which are higher than the reference data at  $z = 1.0H$ . Close to neutral ( $-z'/L < 0.01$ ) values become very large with increased scatter which could be an artifact of very small  $T_*$  values used in the denominator of Eq. 4.

Tables 4 and 5 summarize RMS values of  $\log(\phi_\epsilon)$  and  $\log(\phi_{CT})$  in fitting the various MOS functions to the observed data. The stability range for fitting was chosen as  $0.01 < -z'/L < 2$  to coincide with the various ranges of the available MOS functions. Tables 4 and 5 together with Figs. 4 and 5 suggest guidelines for choosing MOS functions in the urban RSL for the SL approach. Within the internal boundary layer generated by the trailing edge of a building, i.e., above canyons, the function for the canyon case in R06 is closest to the measured data (lowest RMS values in Table 4). Exception is  $z = 2H$  for both  $\phi_\epsilon$  and  $\phi_{CT}$  where the RO06 roof-top function performs better. The situation is less clear in the internal boundary layer formed at the upwind edge of buildings (i.e., above roof-tops). Overall, the RO06 roof-top function provides the best results (lowest RMS values in Table 5) for both  $\phi_\epsilon$  and  $\phi_{CT}$ . Considering only  $\phi_\epsilon$ , the rural reference provides an equally good fit at all heights, but both functions still slightly overpredict the measured data. In the case of  $\phi_{CT}$  at the lowest two heights,

**Table 4** Root mean square (RMS) of  $\log(\phi_\epsilon)$  and  $\log(\phi_{CT})$  between measured values and MOS functions from RO06 (RC canyon case,  $z = 1.01H$ ; RR rooftop case,  $z = 1.32H$ ), KA02 (KA  $z = 2.62H$  and  $3.8H$ ) and rural reference from TG92 (rural) at the canyon location for  $0.01 < -z'/L < 2$

Location	RC	RR	KA	rural	N
$\phi_\epsilon$					
canyon 2H	0.51	0.34	0.54	0.37	97
canyon 1.5H	0.36	0.41	0.46	0.42	93
canyon 1.25H	0.30	0.49	0.44	0.49	117
canyon 1.0H	0.34	0.53	0.44	0.51	90
$\phi_{CT}$					
canyon 2H	1.11	0.98	1.35	1.19	97
canyon 1.5H	0.47	0.61	0.73	0.54	93
canyon 1.25H	0.31	0.80	0.49	0.31	117
canyon 1.0H	0.41	0.59	0.83	0.54	90

N number of 30-min runs

Cells with lowest RMS values have gray shading

**Table 5** Same as Table 4 but for the roof-top location

Location	RC	RR	KA	rural	N
$\phi_\epsilon$					
roof-top 2H	0.48	0.38	0.41	0.37	54
roof-top 1.5H	0.41	0.31	0.42	0.32	57
roof-top 1.25H	0.65	0.39	0.54	0.38	45
roof-top 1.125H	0.44	0.30	0.41	0.29	46
$\phi_{CT}$					
roof-top 2H	0.80	0.65	1.16	0.91	54
roof-top 1.5H	1.17	1.04	1.41	1.24	57
roof-top 1.25H	0.38	0.61	0.75	0.48	45
roof-top 1.125H	0.42	0.46	0.82	0.55	46

the canyon function from RO06 fits best within the stability range considered.

### 6 Evaluation of fluxes

The fluxes of momentum and sensible heat obtained by the two approaches of EC and SL (using Eqs. 5 and 6 for SL based on above evaluation) are compared against each other in Fig. 6. Generally, very good agreement was found for  $u_*$  at all heights. The slight underestimation by the SL approach is a result of underestimating  $\epsilon$  (Fig. 2). SL slightly overestimated  $Q_H$  although the values are relatively small ( $< 100 \text{ Wm}^{-2}$ ) and in some cases close to the instrumental limits ( $10\text{--}30 \text{ Wm}^{-2}$ , Aubinet et al. 2014) which can cause problems in measurement accuracy. Similar overestimation of  $Q_H$  was found in RO06 for  $Q_H < 50 \text{ Wm}^{-2}$  and is likely due to an overestimation of  $C_T^2$  (Fig. 2). This effect is largest at  $z = 1.0H$  and  $2.0H$ , possibly due to larger horizontal temperature gradients at these two locations as explained above, and at  $z = 1.0H$  because of difficulties to determine an appropriate  $d$  value (see below).  $u_*$  is not affected in the same way because  $C_T^2$  influences  $Q_H$  more than  $u_*$ . If  $C_T^2$  is decreased by 20 % (red symbols in Fig. 6), the two methods agree much better, suggesting potential for improvement. One exception is  $1.0H$ , where  $Q_H$  from the  $0.8C_T^2$  calculation is still overestimated. This could be due to a wrong choice for  $d$ . Christen et al. (2004) suggested that  $d$  within the canyon is half the canyon width, i.e.,  $0.75 \text{ m}$  at the present site. As shown by the sensitivity analysis for  $d$  below, this would result in very good agreement between the two approaches (but make it slightly worse for  $u_*$ ) (Table 6). Another possibility for the disagreement in  $Q_H$  is that EC, unlike SL, does not measure the dispersive flux which is more

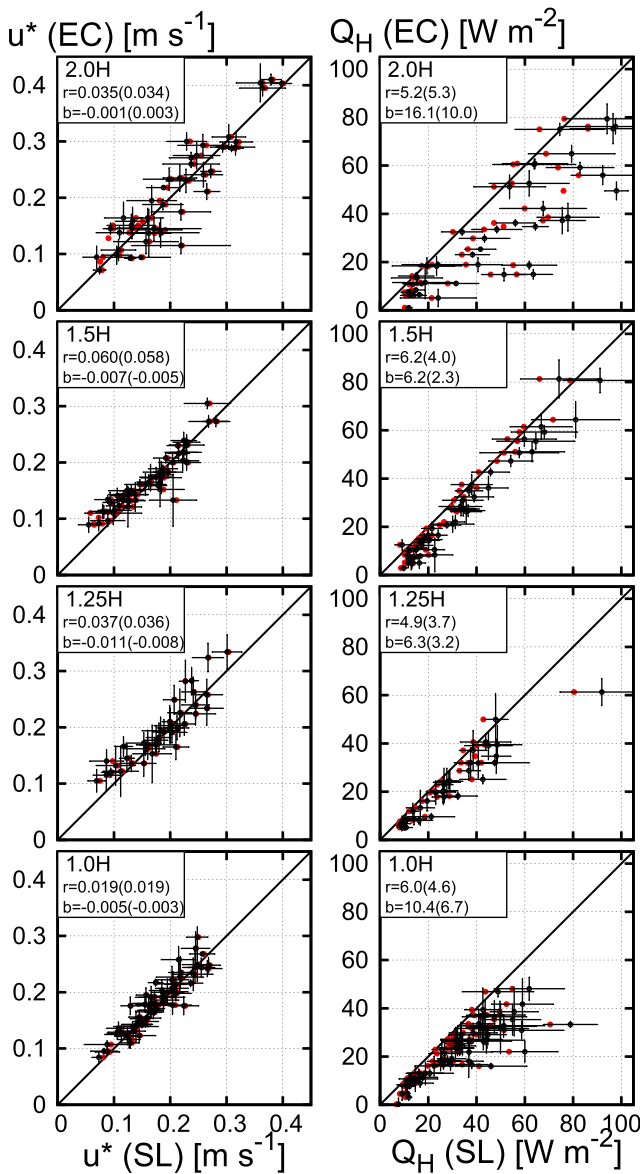


**Fig. 6** Same as Fig. 2 but for friction velocity,  $u_*$  (momentum flux) and sensible heat flux,  $Q_H$ . Black and red symbols are reference and  $C_T^2$ -20% case, respectively (see text).  $r$  is root mean square in  $\text{m s}^{-1}$  and  $\text{W m}^{-2}$  calculated as  $u_*(EC) - u_*(SL)$  and  $Q_H(EC) - Q_H(SL)$ , respectively, for the reference ( $C_T^2$ -20%) case.  $b$  is mean bias error in  $\text{m s}^{-1}$  and  $\text{W m}^{-2}$

**Table 6** Percentage change in momentum ( $u_*$ ) and sensible heat ( $Q_H$ ) fluxes compared to reference case ( $d = 1.15 \text{ m}$ ; MOS functions in Eqs 5 and 6) at 1.0H above the canyon

	$\epsilon$		$C_T^2$		$d$	MOS		
	+8 %	-20 %				Rural	RR	KA
$u_* [\text{ms}^{-1}]$	3.3	1.6	-18.5	-12.6	-13.3	-3.0		
$Q_H [\text{Wm}^{-2}]$	2.2	-11.3	-41.7	-13.8	-16.5	3.6		

Changes include 8% increase in  $\epsilon$ , 20% decrease in  $C_T^2$ , decreasing  $d$  to 0.72 m and application of alternate MOS functions: rural, RR, and KA are Eqs. 7–8, 9–10, and 11–12, respectively

important in the case of the sensible heat than momentum flux (Inagaki et al. 2011).

The momentum and heat fluxes determined using the SL approach depend on  $\epsilon$ ,  $C_T^2$ ,  $d$ , and choice of the MOS function. The sensitivity of the fluxes to these variables is evaluated using data at 1.0H at the canyon location (Table 6). The reference case is calculated using measured  $\epsilon$  and  $C_T^2$ , the MOS functions in Eqs. 5 and 6 which showed the lowest RMS values in Table 4 and  $d = 1.15 \text{ m}$ . To evaluate realistic variations of the fluxes,  $\epsilon$  and  $C_T^2$  were varied by +8 and -20%, respectively, according to the underestimation and overestimation seen in Fig. 2. MOS functions for the urban RSL (Eqs. 7, 8 and 9, 10) and for a flat, homogeneous surface (Eqs. 11 and 12) were tested, together with a different zero-plane displacement length (0.72 m).

The fluxes are very sensitive to the choice of  $d$  (Table 6). This result demonstrates the importance of the proper estimation of this parameter. Morphometric approaches are widely used for estimation of  $d$ , although their values of  $d$  could vary (Table 1) even for the regularly aligned same-size cubes in the COSMO site. Comprehensive comparison for several morphometric methods in Grimmond and Oke (1999) suggested a practical guideline for choice of the method in urban area. Kanda et al. (2013) presented the method for the urban canopy with building-height variation. The influence of  $d$  on  $Q_H$  is larger compared to  $u_*$  because the slope of  $\phi_{CT}$  is steeper than that of  $\phi_\epsilon$  for the stability range encountered during the present study (evaluated at  $z^*/L \approx -0.04$ ). During higher instability when  $\phi_\epsilon$  is steeper,  $u_*$  will be more sensitive to changes in  $d$ . Changes in  $\epsilon$  affect  $u_*$  and  $Q_H$  to similar degrees, on the other hand,  $C_T^2$  primarily influences  $Q_H$  because its influence on  $u_*$  is only indirect through  $z^*/L$ . Sensitivity to two alternative MOS functions suggested in the literature for the urban atmosphere (Eqs. 7–8 and 9–10) is quite different (Table 6). Although this comparison depends on the stability range, the choice of MOS function is of secondary importance in SL calculations when compared to  $d$ .

### 7 Summary and conclusion

Scintillometry measurements of turbulent fluxes have the potential to provide area-averaged fluxes in the urban RSL. The present study evaluated scintillometry measurements of  $\epsilon$  and  $C_T^2$ , as well as the final product of momentum and heat fluxes against the spatial average of four sonic anemometers aligned along the path of the scintillometer. Experiments were carried out above an array of regular cubes at four heights between  $z = 1.0H$  and  $2.0H$ .

The values of  $\epsilon$  ( $C_T^2$ ) from the scintillometer showed slight under- (over-) estimation compared to those obtained from the spectral energy density in the inertial subrange of the sonic anemometers. However, differences were within the spatial



variation of the four sonic anemometers and the temporal variation of the scintillometer signal within the 30-min averaging period.

$Q_H(u_*)$  from SL agreed well with that from EC. The scintillometer calculation of fluxes strongly depends on the zero-plane displacement length and the form of the similarity function. A sensitivity analysis showed that these two factors have a larger effect on resulting fluxes than errors in the raw data ( $\varepsilon$  and  $C_T^2$ ).

Similarity functions ( $\phi_\varepsilon$  and  $\phi_{CT}$ ) for urban roughness sublayers developed in previous urban studies were compared to those from the present sonic anemometer measurements. In the internal boundary layer formed at the leading edge of the roughness tops (roofs), the measured  $\phi_\varepsilon$  and  $\phi_{CT}$  showed best agreement with functions developed over building roofs in RO06, and in the case of  $\phi_\varepsilon$  for a flat homogeneous surface by TG92, surprisingly throughout the entire RSL. This result, together with the finding that both functions overpredict the measured values, points to the need for additional research. On the other hand, in the internal boundary layer developing at the downwind edge of the cube including the space above the canyon, the functions are close to those previously developed above the canyon-top in RO06. The values of  $\phi_\varepsilon$  and  $\phi_{CT}$  approach those for the rural reference at the upper measurement levels at  $z = 1.5 H$  and  $2.0H$ . The present study provides further guidelines for choosing SL similarity functions in the urban RSL.

**Acknowledgments** The scintillometer measurements were facilitated by Dr. Ken-ichi Narita (Nippon Institute of Technology), Dr. Tsuyoshi Honjo (Chiba University), and Dr. Tsuyoshi Tada (National Defense Academy of Japan).

## References

- Aubinet M, Vesala T, Papale D (eds) (2014) Eddy covariance. Springer, Sordrecht, 438pp
- Bottema M (1997) Urban roughness modelling in relation to pollutant dispersion. *Atmos Environ* 31:3059–3075
- Christen A, Rotach MW, Vogt R (2004) Experimental determination of the urban kinetic energy budget within and above an urban canyon. Proceedings, Fifth Symposium on the Urban Environment. Vancouver, Canada, August 23–26, 2004, American Meteorological Society, 45 Beacon St., Boston, MA, (CD-ROM)
- Christen A, Rotach MW, Vogt R (2009) The budget of turbulent kinetic energy in the urban roughness sublayer. *Bound -Layer Meteorol* 131:193–222
- De Bruin HAR, Meijninger WML, Smedman AS, Magunusson M (2002) Displaced-beam small aperture scintillometer test. part I: the WINT EX data-set. *Bound -Layer Meteorol* 105:129–148
- Frehlich R (1992) Laser Scintillation measurements of the temperature spectrum in the atmospheric surface layer. *J Atmos Sci* 49:1494–1509
- Grimmond CSB, Oke TR (1999) Aerodynamic properties of urban areas derived from analysis of surface form. *J Appl Meteorol* 38:262–1292
- Hartogensis OK, De Bruin HAR, Van De Wiel BJH (2002) Displaced-beam small aperture scintillometer test. part II: cases-99 stable boundary-layer experiment. *Bound -Layer Meteorol* 105:149–176
- Hill RJ (1978) Models of the scalar spectrum for turbulent advection. *J Fluid Mech* 88:541–562
- Inagaki A, Kanda M (2008) Turbulent flow similarity over an array of cubes in near-neutrally stratified atmospheric flow. *J Fluid Mech* 615:101–120
- Inagaki A, Castillo MCL, Yamashita Y, Kanda M, Takimoto H (2011) Large-eddy simulation of coherent flow structures within a cubical canopy. *Bound -Layer Meteorol* 142:207–222
- Kanda M, Moriwaki R, Roth M, Oke T (2002) Area-averaged sensible heat flux and a new method to determine zero-plane displacement length over an urban surface using scintillometry. *Bound -Layer Meteorol* 105:177–193
- Kanda M, Kanega M, Kawai T, Moriwaki R, Sugawara H (2007) Roughness lengths for momentum and heat derived from outdoor urban scale models. *J Appl Climatol* 46:1067–1079
- Kanda M, Inagaki A, Miyamoto T, Gryschka M, Raasch S (2013) A new aerodynamic parametrization for real urban surfaces. *Bound -Layer Meteorol* 147:357–377
- Lagouarde JP, Irvine M, Bonnefond JM, Grimmond CSB, Long N, Oke TR, Salmond JA, Offerle B (2005) Monitoring the sensible heat flux over urban areas using large aperture scintillometry: case study of Marseille city during the ESCOMPTE Experiment. *Bound -Layer Meteorol* 118:449–476
- Macdonald RW, Griffiths RF, Hall DJ (1998) An improved method for the estimation of surface roughness of obstacle arrays. *Atmos Environ* 32:1857–1864
- Meijninger WML, Hartogensis OK, Kohsiek W, Hoedjes JCB, Zuurbier RM, De Bruin HAR (2002) Determination of area-averaged sensible heat fluxes with a large aperture scintillometer over a heterogeneous surface -Flevoland field experiment. *Bound -Layer Meteorol* 105: 37–62
- Moriwaki R, Kanda M (2006) Scalar roughness parameters for a suburban area. *J Meteorol Soc Jap* 84:1063–1071
- Rotach MW (1994) Determination of the zero plane displacement in an urban environment. *Bound -Layer Meteorol* 67:187–193
- Roth M (2000) Review of atmospheric turbulence over cities. *Quart J Roy Meteorol Soc* 126:941–990
- Roth M, Salmond JA, Satyanarayana ANV (2006) Methodological considerations regarding the measurement of turbulent fluxes in the urban roughness sublayer: the role of scintillometry. *Bound -Layer Meteorol* 121:351–375
- Roth M, Inagaki A, Sugawara H, Kanda M (2015) Small-scale spatial variability of turbulence statistics, (co)spectra and turbulent kinetic energy measured over a regular array of cube roughness. *Env. Fluid Mech* 15:329–348
- Scintec (2008) Scintec surface layer scintillometer user manual. Scintec AG, 100pp
- Thiermann V, Grassl H (1992) The measurement of turbulent surface-layer fluxes by use of bichromatic scintillation. *Bound -Layer Meteorol* 58:367–389
- Toda M, Sugita M (2003) Single level turbulence measurements to determine roughness parameters of complex terrain. *J Geophys Res* 108(D12):4363. doi:10.1029/2002JD002573
- Van Kesteren B, Beyrich F, Hartogensis OK, van den Kroonenberg AC (2013) The effect of a new calibration procedure on the measurement accuracy of Scintec's displaced-beam laser scintillometer. *Bound -Layer Meteorol* 151:257–271
- Ward HC, Evans JG, Grimmond CSB (2014) Multi-scale sensible heat fluxes in the suburban environment from large-aperture scintillometry and eddy covariance. *Bound -Layer Meteorol* 152: 65–89